

# Active Galactic Nucleus and Extended Starbursts in a Mid-stage Merger VV114

Daisuke IONO<sup>1,2</sup>, Toshiaki SAITO<sup>1,3</sup>, Min S. YUN<sup>4</sup>, Ryohei KAWABE<sup>1,5</sup>, Daniel ESPADA<sup>1,5</sup>, Yoshiaki HAGIWARA<sup>1,2</sup>, Masatoshi IMANISHI<sup>1,2</sup>, Takuma IZUMI<sup>6</sup>, Kotaro KOHNO<sup>6,7</sup>, Kentaro MOTOHARA<sup>6</sup>, Koichiro NAKANISHI<sup>2,5</sup>, Hajime SUGAI<sup>8</sup>, Ken TATEUCHI<sup>6</sup>, Yoichi TAMURA<sup>6</sup>, Junko UEDA<sup>1,3,9</sup>, Yuzuru YOSHII<sup>6</sup>

<sup>1</sup>National Astronomical Observatory of Japan, 2-21-1 Osawa, Mitaka, Tokyo 181-8588

<sup>2</sup>The Graduate University for Advanced Studies (SOKENDAI), 2-21-1 Osawa, Mitaka, Tokyo 181-0015

<sup>3</sup>Department of Astronomy, School of Science, The University of Tokyo, 7-3-1 Hongo, Bunkyo-ku, Tokyo 133-0033

<sup>4</sup>Department of Astronomy, University of Massachusetts, Amherst, MA 01003

<sup>5</sup>Joint ALMA Observatory, Alonso de Cordova 3107, Vitacura, Santiago 763-0355, Chile

<sup>6</sup>Institute of Astronomy, University of Tokyo, 2-21-1 Osawa, Mitaka, Tokyo 181-0015

<sup>7</sup>Research Center for the Early Universe (WPI), University of Tokyo, 7-3-1 Hongo, Bunkyo, Tokyo 113-0033, Japan

<sup>8</sup>Kavli Institute for the Physics and Mathematics of the Universe, The Univ. of Tokyo

<sup>9</sup>Harvard-Smithsonian Center for Astrophysics, 60 Garden Street, Cambridge, MA 02138

(Received ; accepted )

## Abstract

High resolution ( $\sim 0''.4$ ) Atacama Large Millimeter/submillimeter Array (ALMA) Cycle 0 observations of HCO<sup>+</sup>(4–3) and HCN (4–3) toward a mid-stage infrared bright merger VV 114 have revealed compact nuclear ( $< 200$  pc) and extended ( $\sim 3 - 4$  kpc) dense gas distribution across the eastern part of the galaxy pair. We find significant enhancement of HCN (4–3) emission in an unresolved compact and broad ( $290 \text{ km s}^{-1}$ ) component found in the eastern nucleus of VV114, and we suggest dense gas associated with the surrounding material around an Active Galactic Nucleus (AGN), with a mass upper limit of  $\lesssim 4 \times 10^8 M_{\odot}$ . The extended dense gas is distributed along a filamentary structure with resolved dense gas concentrations ( $\sim 230$  pc;  $\sim 10^6 M_{\odot}$ ) separated by a mean projected distance of  $\sim 600$  pc, many of which are generally consistent with the location of star formation traced in Pa $\alpha$  emission. Radiative transfer calculations suggest moderately dense ( $n_{\text{H}_2} = 10^5 - 10^6 \text{ cm}^{-3}$ ) gas averaged over the entire emission region. These new ALMA observations demonstrate the strength of the dense gas tracers in identifying both the AGN and star formation activity in a galaxy merger, even in the most dust enshrouded environments in the local universe.

**Key words:** telescopes — galaxies:evolution — galaxies:starburst — galaxies:interactions

## 1. Introduction

Cosmological simulations have clearly established that galaxy collisions and mergers play major roles in the formation and evolution of galaxies by triggering a rapid mass build-up (e.g., Cole et al. 2000). High-resolution major merger simulations have shown that the star formation physics is more dominated by mass fragmentation and turbulent motion across the merging disks, forming massive clumps of dense gas clouds ( $M_{\text{gas}} = 10^{6-8} M_{\odot}$ ) and triggering star formation across the galaxy disks (Teyssier et al. 2010), or in a dense filamentary structure along the merging interface (Saitoh et al. 2009). In some cases, radial streaming can efficiently feed the gas to the central black hole, possibly triggering an ‘AGN phase’ during the course of the galaxy merger evolution (e.g. Hopkins et al. 2006).

An important observational test is to map the dense gas tracers in merging U/LIRGs (Ultra Luminous Infrared Galaxies) since they show high degree of starburst activity, some of which harbor AGNs in their centers (Sanders & Mirabel 1996). The HCN (4–3) and HCO<sup>+</sup>(4–3) emis-

sion, whose critical densities are  $n_{\text{crit}} \sim 2 \times 10^7 \text{ cm}^{-3}$  and  $n_{\text{crit}} \sim 4 \times 10^6 \text{ cm}^{-3}$  (Meijerink et al. 2007) respectively, are both reliable dense gas tracers and now readily accessible at sub arcsecond angular resolution with the advent of the Atacama Large Millimeter/Submillimeter Array (ALMA). Here we present ALMA Cycle 0 HCN (4–3) and HCO<sup>+</sup>(4–3) observations of an IR-bright galaxy VV114 with the primary goal to study the distribution of dense gas during the critical stage when the two gas rich galaxies collide and merge.

VV114 is a gas-rich ( $M_{\text{H}_2} = 5.1 \times 10^{10} M_{\odot}$ ; Yun et al. 1994, Iono et al. 2004 and Wilson et al. 2008) interacting pair with high-infrared luminosity ( $L_{\text{IR}} = 4.0 \times 10^{11} L_{\odot}$ ) located at  $D = 86$  Mpc ( $1'' = 0.4$  kpc). It consists of two optical galaxies (VV114E and VV114W) with a projected separation of 6 kpc (Figure 1). Evidence for wide-spread star formation activity and shocks across the entire system is found in the UV, optical, and mid-IR (Alonso-Herrero et al. 2002, Goldader et al. 2002, Rich et al. 2011). A dust-obscured AGN in VV114E is also suggested (but not conclusive) from NIR (Le Floch et al. 2002; Imanishi et al. 2007) and X-ray observations (Grimes et al. 2006), sug-

gesting that both starburst and AGN activities might have been triggered by the ongoing merger.

## 2. ALMA Observations

The HCN (4–3) ( $\nu_{rest} = 354.505$  GHz) and HCO<sup>+</sup>(4–3) ( $\nu_{rest} = 356.734$  GHz) observations toward VV114 were obtained on June 1 – 3, 2012 during the Cycle 0 program of ALMA using the extended configuration. The digital correlator was configured with 0.488 MHz resolution for the spectral window that contains the emission lines. Absolute flux calibration was performed using Uranus, J1924-292 was used for bandpass calibration, and the time dependent gain calibration was performed using J0132-169 (6 degrees away from VV 114). The total on source time was 86 minutes.

We used the delivered calibrated data product and CLEANed the image down to 1.5 sigma using the ALMA data reduction package CASA. Channel maps with 30 km s<sup>-1</sup> velocity resolution were made, with a synthesized beam size of 0.''5 × 0.''4 (PA = 52 degrees)(equivalent to 200 × 160 pc). The rms noise level was 0.9 mJy beam<sup>-1</sup> for the robust=0.5 maps. The continuum was subtracted using all of the line-free channels in the bandpass.

## 3. Distribution of HCN (4–3) and HCO<sup>+</sup>(4–3)

The HCN (4–3) and HCO<sup>+</sup>(4–3) integrated intensity maps are presented in Figure 1. While the HCN (4–3) emission is only seen near the eastern nucleus of VV114 and resolved into four peaks, the HCO<sup>+</sup>(4–3) emission is more extended and has at least 10 peaks in the integrated intensity map. The total integrated intensity of HCO<sup>+</sup>(4–3) and HCN (4–3) are  $15.3 \pm 0.4$  Jy km s<sup>-1</sup> and  $4.4 \pm 0.2$  Jy km s<sup>-1</sup>, respectively. The higher HCO<sup>+</sup>(4–3) flux observed by the SMA ( $\geq 17 \pm 2$  mJy; Wilson et al. 2008) using a 2.''8 × 2.''0 beam is likely attributed to missing flux by the ALMA observation. We show a direct comparison between the J=4–3 (this work) and J=1–0 (taken at the Nobeyama Millimeter Array; Imanishi et al. (2007)) transitions of both species in Figure 2, after convolving the ALMA images with the NMA beam (7.''5 × 5.''5). While the J=4–3 transitions of both species are concentrated near the eastern near-infrared nucleus with a slight extension to the west for HCO<sup>+</sup> (4–3), the distribution of the HCN (1–0) and HCO<sup>+</sup> (1–0) are different; the HCN (1–0) emission is separated into two clumps in the east-west whereas the HCO<sup>+</sup> (1–0) emission is extended widely toward the western nucleus.

We label the six HCO<sup>+</sup>(4–3) peaks in the eastern part of VV114 as E0 – E5 and the four detected in the western part of VV114 as W0 – W3 (Figure 1, Table 1). The HCO<sup>+</sup>(4–3) and HCN (4–3) emission peaks are spatially consistent for E0 – E3. The compact component E0 is unresolved with the current resolution, and the size upper limit is < 200 pc. HCN (4–3) emission is not detected in the overlap region (W0 – W2), where the high CO (1–0) velocity dispersion and significant methanol detection both suggest the presence of shocked gas (Saito et al. in

preparation).

## 4. Dense Gas and AGN /Starburst Activity

### 4.1. Relative Strengths of HCN (4–3) and HCO<sup>+</sup>(4–3) and a Signature of AGN

We present a comparison between the surface brightness of HCO<sup>+</sup>(4–3) and HCN (4–3) in Figure 3. Although the statistics are limited, the three molecular clumps (E1, E2 and E3) show an increasing trend between  $\Sigma_{\text{HCN}}$  and  $\Sigma_{\text{HCO}^+}$ . In contrast, the ratio between the beam averaged surface brightness of E0 is a factor of three higher than E1, E2 and E3; E0 is the only component that has HCN (4–3) – HCO<sup>+</sup>(4–3) integrated flux ratio which is larger than unity (HCN (4–3)/HCO<sup>+</sup>(4–3) = 1.6). Gaussian fits to the HCO<sup>+</sup>(4–3) and HCN (4–3) spectra at E0 give peak = 9.0 mJy,  $\sigma = 123$  km s<sup>-1</sup> (for HCN (4–3)) and peak = 6.9 mJy,  $\sigma = 93$  km s<sup>-1</sup> (for HCO<sup>+</sup>(4–3)). Thus the HCN (4–3) emission is not only brighter at E0, but it is also broader than the gas traced in HCO<sup>+</sup>(4–3), suggesting that the HCN (4–3) and HCO<sup>+</sup>(4–3) are tracing physically different gas at < 200 pc scales. Such a high relative intensity of the HCN emission is possibly a signature of a buried AGN, as suggested by previous studies (e.g. Kohno et al. 2001).

It has been known that the brightness of the HCN emission line is enhanced near the AGN compared to star forming regions (Kohno et al. 2001), with higher contrast in high J transitions (Hsieh et al. 2012). Individual galaxies (e.g. NGC 1068, NGC 1097) have been studied extensively in high resolution (Kohno et al. 2003, Krips et al. 2011, Hsieh et al. 2012), clearly revealing the over abundance of HCN emission near the Seyfert nucleus, through J = 1 to 4. The exact reasoning for the enhanced intensity ratio is not clearly understood, and it could be due to gas excitation effects (e.g. density and temperature), intensity of the incident radiation field (e.g. PDR vs. XDR), IR pumping (e.g. Garcia-Burillo et al. 2006), or other non-collisional excitation due to star formation or supernovae explosions (see Krips et al. 2008 for a discussion). There is evidence suggesting the dominance of low density (< 10<sup>4.5</sup> cm<sup>-3</sup>) gas in a sample of AGNs (Krips et al. 2008), and hence the difference in critical density is likely not the only reason for the difference in the relative abundance.

Regardless of the exact physical origin of the higher relative intensity of the HCN (4–3) emitting gas, the broad (FWHM = 290 km s<sup>-1</sup>) and compact (< 200 pc) unresolved source E0 is of significant interest, since it coincides with the region where past observations suggest the presence of a buried AGN. We derive the upper limit to the dynamical mass by using  $M_{\text{dyn}} = r\sigma^2/G$  (assuming an inclination of 90 degrees for simplicity), where  $r$  is the radius enclosing the emission region,  $\sigma$  is the width of the HCN line, and  $G$  is the gravitational constant. The upper limit to the dynamical mass estimated from the line-width and the beam size is  $\lesssim 4 \times 10^8 M_{\odot}$ . Since the HCN emission is generally believed to be optically thick, we estimate the dense gas mass of the E0 component adopting

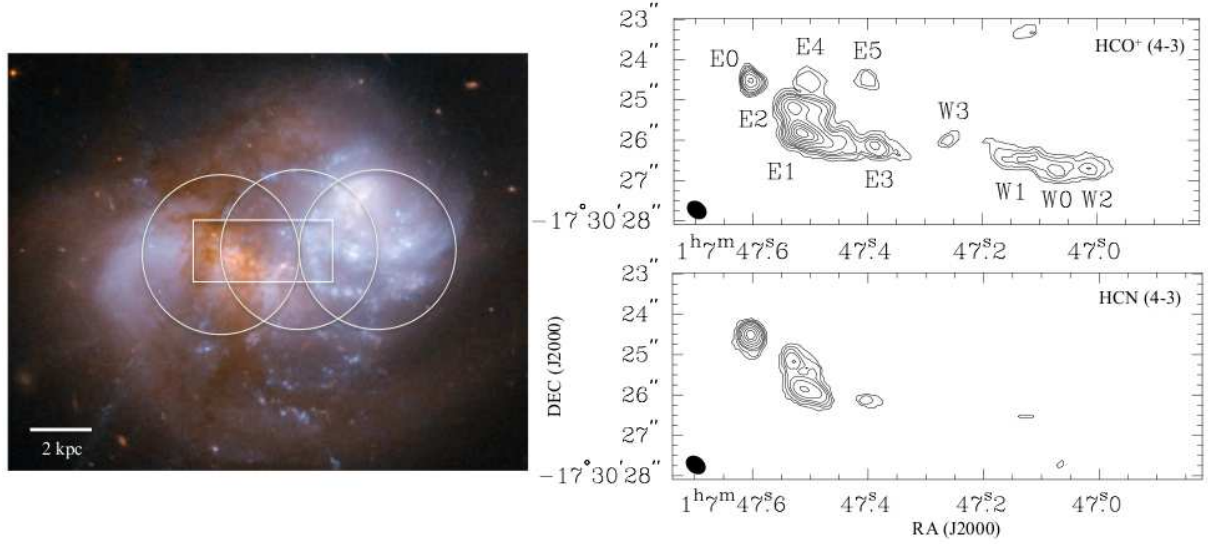


**Fig. 1.** (left) HST ACS image of VV114 overlaid with the approximate regions of the panels shown on the right, and the approximate field of views of the ALMA 3-point mosaic. (Credit: NASA, ESA, the Hubble Heritage (STScI/AURA)-ESA/Hubble Collaboration, and A. Evans (University of Virginia, Charlottesville/NRAO/Stony Brook University). (right) The distribution of  $\text{HCO}^+$  (4–3) (top) and  $\text{HCN}$  (4–3) (bottom) in VV 114. The contours are; 0.05, 0.15, 0.25, 0.35, 0.55, 0.85, 1.25, 1.65, 2.05, 2.45  $\text{Jy km s}^{-1}$ .

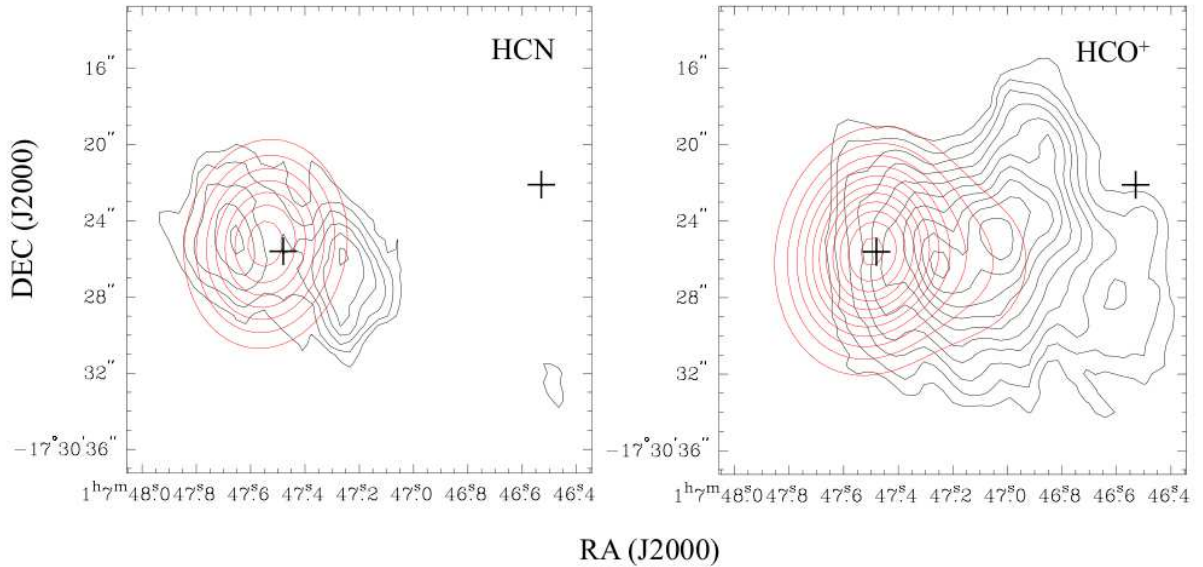


**Fig. 2.** (left) The  $\text{HCN}$  (1–0) emission (Imanishi et al. 2007; in dark contours) is compared with the  $\text{HCN}$  (4–3) emission convolved to the NMA resolution (in red contours). The contour levels for  $\text{HCN}$  (1–0) are the same as Imanishi et al. (2007) and the  $\text{HCN}$  (4–3) contours are  $(2.8 - 4.8) \times 10^{-2}$  (in steps of  $0.2 \times 10^{-2}$ )  $\text{Jy/beam km s}^{-1}$ . The crosses indicate the locations of the near-infrared peaks shown in Figure 2 of Imanishi et al. (2007). (right) Similar to *left* but for the  $\text{HCO}^+$  emission. The  $\text{HCN}$  (4–3) contours are  $(1.0 - 1.7) \times 10^{-2}$  (in steps of  $0.1 \times 10^{-2}$ )  $\text{Jy/beam km s}^{-1}$ .

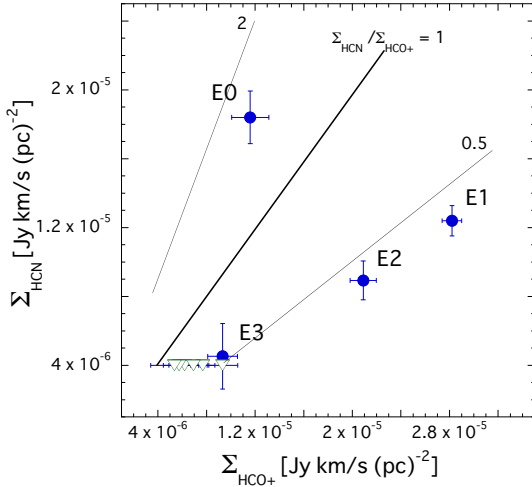


**Fig. 3.** Relation between the HCN (4–3) and  $\text{HCO}^+(4-3)$  surface brightness for different regions in VV114. The triangles represent upper limits to the HCN (4–3) surface brightness. The solid lines are the surface brightness ratio of 0.5, 1 and 2.

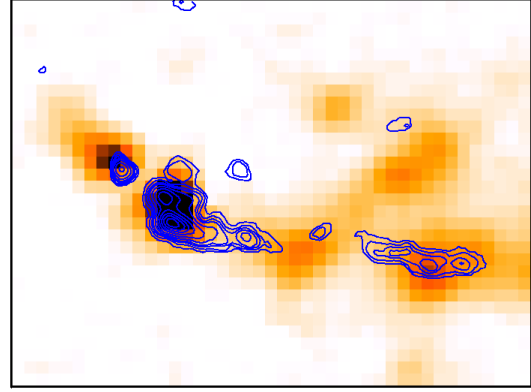


**Fig. 4.**  $\text{HCO}^+(4-3)$  emission overlaid on a  $\text{Pa}\alpha$  image. The contour levels are the same as Figure 1. The  $\text{Pa}\alpha$  map (Tateuchi et al. 2012) is obtained using the NIR camera ANIR (Motohara et al. 2008) mounted on the University of Tokyo Atacama Observatory 1m telescope (miniTAO) (Minezaki et al. 2010). A  $\sim 1$  kpc long  $\text{Pa}\alpha$  extension to the NE is also seen emanating from the putative AGN, which may be a signature of shock ionization, or star formation activity in the compressed gas along the AGN jet.

the conversion factor provided in Gao & Solomon (2004). Using the integrated intensity of HCN (4–3) (see Section 3) and  $\text{HCN}(1-0) = 7 \text{ Jy km s}^{-1}$  (Imanishi et al. 2007), we derive  $\text{HCN}(4-3)/(1-0) = 0.63$ . This yields a dense gas mass of  $\sim 8.1 \times 10^6 M_\odot$ , hence  $> 2\%$  of the total mass is in dense molecular form and significant amount of dense gas is present in a very compact region.

Finally, we note that while these are evidences suggesting a compact AGN near the eastern nucleus of VV114, the 350 GHz – 8.5 GHz flux ratio suggests the contrary. The ratio is  $1.2 \pm 0.1$  for E0, and  $1.1 \pm 0.1$  for E1 and E2, using the the archival 8.5 GHz radio continuum image obtained from the VLA archive (beam size  $\sim 0''.9$ ) and the 350 GHz image obtained from the ALMA observations. The 350 GHz continuum emission is also unresolved at E0, but E1 and E2 show resolved structure. If the dominant source of radio continuum emission is indeed due to hot plasma surrounding the AGN, then we expect this ratio to be higher near the putative AGN (i.e. E0), which is inconsistent with the current results and argues in favor of a common physical origin (e.g. a massive starburst) in all three regions. Higher resolution radio continuum imaging is necessary to understand the origin of the radio emission in E0.

#### 4.2. Extended Dense Gas Filament, Star Formation, and the Global Gas Conditions

The average size of the clumps forming the filamentary structure (i.e. E1–E5, W0–W3) is  $230 \pm 70$  pc, with an average dense gas mass of  $\sim 10^6 M_\odot$  and a mean projected separation of  $\sim 600$  pc. We compare the distribution of the  $\text{HCO}^+(4-3)$  and star formation activity traced in  $\text{Pa}\alpha$  line in Figure 4. Spatial correspondence between  $\text{HCO}^+(4-3)$  and the brightest peaks of  $\text{Pa}\alpha$  is generally seen. Such a long filamentary dense gas structure and associated star formation are predicted along the colliding interface of

two colliding galaxies (Saitoh et al. 2009), and the masses are also consistent with the massive star forming clumps predicted in simulations by Teyssier et al. (2010).

Finally, we derive the global physical conditions of gas by comparing the total integrated  $\text{HCO}^+(4-3)/(1-0)$  and  $\text{HCN}(4-3)/(1-0)$  ratios to the results from radiative transfer modeling (RADEX; Van der Tak et al. 2007). The results are  $n_{\text{H}_2} = 10^5 - 10^6 \text{ cm}^{-3}$  and  $T = 30 - 500$  K, assuming abundance ratios of  $[\text{HCO}^+]/[\text{H}_2] = 1.0 \times 10^{-9}$  (Irvine et al. 1987) and  $[\text{HCN}]/[\text{HCO}^+] = 0.1$  to 1 (to be consistent with M82; Krips et al. 2008). Although the range in the derived temperature is too large to be a meaningful constraint, this suggests the presence of moderately dense gas averaged over the entire galaxy pair. We caution here that these are average quantities which are derived without considering the difference in the spatial distribution between the J=4–3 and 1–0 transitions (see Figure 2). Higher angular resolution imaging of the J=1–0 transition is clearly needed in order to determine the spatial distribution of the physical properties.

## 5. Summary and Future Prospects

We present  $0''.4$  resolution HCN (4–3) and  $\text{HCO}^+(4-3)$  observations toward a mid-stage IR bright merger VV114 obtained during cycle 0 program of ALMA. For the first time, these new high-quality maps allow us to investigate the central regions of this merging LIRG at 200 pc resolution. We find that both the HCN (4–3) and  $\text{HCO}^+(4-3)$  emission in the eastern nucleus of VV 114 are compact ( $< 200$  pc) and broad ( $290 \text{ km s}^{-1}$  for HCN (4–3)) with high HCN (4–3)/ $\text{HCO}^+(4-3)$  ratio. From the new ALMA observations along with past X-ray and NIR observations, we suggest the presence of an obscured AGN in the eastern nucleus of VV114. We also detect a 3–4 kpc long fil-



**Table 1.** Properties of the Molecular Clumps

| Source | $S_{\text{HCO}^+} \text{ dv}^1$<br>[Jy km/s] | $S_{\text{HCN}} \text{ dv}^1$<br>[Jy km/s] | $T_{\text{HCO}^+}^2$<br>[K] | $T_{\text{HCN}}^2$<br>[K] |
|--------|--|--|-----------------------------|---------------------------|
| E0     | $1.12 \pm 0.15$                              | $1.79 \pm 0.15$                            | 0.40                        | 0.57                      |
| E1     | $7.40 \pm 0.21$                              | $1.82 \pm 0.13$                            | 1.33                        | 0.63                      |
| E2     | $3.06 \pm 0.16$                              | $0.64 \pm 0.08$                            | 0.92                        | 0.44                      |
| E3     | $0.89 \pm 0.12$                              | $0.11 \pm 0.05$                            | 0.35                        | 0.22                      |
| E4     | $0.31 \pm 0.07$                              | –  | 0.30                        | –                         |
| E5     | $0.20 \pm 0.04$                              | –  | 0.24                        | –                         |
| W0     | $0.83 \pm 0.11$                              | –  | 0.37                        | –                         |
| W1     | $0.88 \pm 0.11$                              | –  | 0.26                        | –                         |
| W2     | $0.48 \pm 0.09$                              | –  | 0.32                        | –                         |
| W3     | $0.12 \pm 0.04$                              | –  | 0.17                        | –                         |

<sup>1</sup> The integrated flux densities.

<sup>2</sup> The peak temperature of each molecular clump. The error on each value is 0.05 K.

ament of dense gas, which is likely tracing the active star formation triggered by the ongoing merger. In a forthcoming paper, we will present a comprehensive modeling of VV 114 using our new  $^{12}\text{CO}$  (1–0),  $^{13}\text{CO}$  (1–0) and CO (3–2) ALMA observations, as well as a chemical analysis of the nucleus and the overlap region of VV114 (Saito et al. in prep).

The authors thank the anonymous referee for comments that improved the contents of this paper. This paper makes use of the following ALMA data: ADS/JAO.ALMA#2011.0.00467.S. ALMA is a partnership of ESO (representing its member states), NSF (USA) and NINS (Japan), together with NRC (Canada) and NSC and ASIAA (Taiwan), in cooperation with the Republic of Chile. The Joint ALMA Observatory is operated by ESO, AUI/NRAO and NAOJ.

## References

Alonso-Herrero, A., Rieke, G. H., Rieke, M. J., & Scoville, N. Z., 2002, *AJ*, 124, 166

Cole, S., Lacey, C. G., Baugh, C. M., & Frenk, C. S., 2000, *MNRAS*, 319, 168

Gao, Y. & Solomon, P. M., 2004, *ApJ*, 606, 271

Goldader, J. D., Gerhardt, M., Heckman, T. M., Seiber, M., Sanders, D. B., Calzetti, D., & Steidel, C. C. 2002, *ApJ*, 568, 651

Garcia-Burillo, S., et al., *ApJ*, 645, L17

Grimes, J. P., Heckman, T., Hoopes, C., Strickland, D., Aloisi, A., Meurer, G., & Ptak, A. 2006, *ApJ*, 648, 310

Hopkins, P. F., Hernquist, L., Cox, T. J., Di Matteo, T., Robertson, B., & Springel, V. 2006, *ApJS*, 163, 1

Hsieh, P.-Y., Ho, P.T.P., Kohno, K., Hwang, C.-Y., & Matsushita, S. 2012, *ApJ*, 747, 90

Imanishi, M., Nakanishi, K., Yoichi, T., Oi, N., & Kohno, K. 2007, *AJ*, 134, 2366

Iono, D., Ho, P. T. P., Yun, M. S., Matsushita, S., Peck, A. B., & Sakamoto, K. 2004, *ApJL*, 616, 63

Irvine, W. M., Goldsmith, P. F., & Hjalmarsen, A. 1987, *Interstellar processes; Proceedings of the Symposium, Grand Teton National Park, WY, July 1-7, 1986 (A88-14501 03-90)*. Dordrecht, D. Reidel Publishing Co., 1987,

p. 561-609.

Kohno, K., Matsushita, S., Vila-Vilaro, B., Okumura, S. K., Shibatsuka, T., Okiura, M., Ishizuki, S., & Kawabe, R. 2001, *ASPC*, 239, 672

Kohno, K., Ishizuki, S., Matsushita, S., Vila-Vilaro, B., & Kawabe, R. 2003, *PASJ*, 55, 1

Krips, M., Neri, R., Garcia-Burillo, S., Martin, S., Combes, F., Gracia-Carpio, J., & Eckart, A., *ApJ*, 677, 262 2011, *ApJ*, 736, 37

Krips, M., et al., 2011, *ApJ*, 736, 37

Le Floch, E., Charmandaris, V., Laurent, O., Mirabel, I. F., Gallais, P., Sauvage, M., Vigroux, L., & Cesarsky, C., 2002, *A&A*, 391, 417

Minezaki, T., Kato, D., Sako, S., Konishi, M., Koshida, S., Mitani, N., Aoki, T., Doi, M., Handa, T., Ita, Y., Kawara, K., Kohno, K., Miyata, T., Motohara, K., Soyano, T., Tanabe, T., Tanaka, M., Tarusawa, K., Yoshii, Y., Bronfman, L., Ruiz, M. T., Hamuy, M. 2010, *Proceedings of SPIE*, 7733, 773356-1

Motohara, K., Mitani, N., Sako, S., Uchimoto, Y. K., Toshikawa, K., Yamamuro, T., Handa, T., Tanaka, M., Aoki, T., Doi, M., Kawara, K., Kohno, K., Minezaki, T., Miyata, T., Soyano, T., Tanabe, T., Tarusawa, K., Yoshii, Y. 2008, *Proceedings of SPIE*, 7014, 70142T

Meijerink, R., Spaans, M., & Israel, F. P. 2007, *Å*, 461, 793

Rich, J. A., Kewley, L. J. & Dopita, M. A., 2011, *ApJ*, 734, 87

Sanders, D. B. & Mirabel, I. F., 2012, *ARA&A*, 34, 749

Saitoh, T. R., et al., 2009, *PASJ*, 61, 481

Tateuchi, K., et al., 2012, *PKAS*, 27, 297

Teyssier, R., Chapon, D., & Bournaud, F., 2010, *ApJ*, 720, 149

Van der Tak, F. F. S., Black, J. H., Schoier, J. H., Jansen, D. J., van Dishoeck, E. F., 2007, *A&A* 468, 627

Wilson, C. D., Petitpas, G. R., Iono, D., Baker, A. J., Peck, A. B., Krips, M., Warren, B., Golding, J., Atkinson, A., Armus, L., Cox, T. J., Ho, P., Juvella, M., Matsushita, S., Mihos, C. J., Pihlstrom, Y., Yun, M. S., 2008, *ApJS*, 178, 189L

Yun, M. S., Scoville, N. Z., & Knop, R. A., 1994, *ApJ*, 430, 109L